Model of Electronic Structure and Superconductivity in Orbitally Ordered FeSe

Shantanu Mukherjee,[1] A. Kreisel,[1] P. J. Hirschfeld,[2] and Brian M. Andersen[1]
[1]*Niels Bohr Institute, University of Copenhagen, Universitetsparken 5, DK-2100 Copenhagen, Denmark*
[2]*Department of Physics, University of Florida, Gainesville, Florida 32611, USA*
(Received 11 February 2015; published 8 July 2015)

We provide a band structure with low-energy properties consistent with recent photoemission and quantum oscillation measurements on FeSe, assuming mean-field-like site- and/or bond-centered ferro-orbital ordering at the structural transition. We show how the resulting model provides a consistent explanation of the temperature dependence of the measured Knight shift and the spin-relaxation rate. Furthermore, the superconducting gap structure obtained from spin-fluctuation theory exhibits nodes on the electron pockets, consistent with the V-shaped density of states obtained by tunneling spectroscopy on this material, and the temperature dependence of the London penetration depth.

DOI: 10.1103/PhysRevLett.115.026402 PACS numbers: 71.18.+y, 74.20.Rp, 74.25.Jb, 74.70.Xa

The electronic properties and the nature of the interactions that drive the low-energy physics and the ordered phases of iron-based superconductors (FeSC) continue to pose an outstanding problem in modern condensed matter physics. The diversity of the properties among the different families of FeSC and their complex multiorbital band structure have hindered the understanding of the electronic states in these materials, as well as the mechanism of superconductivity.

A material that stands out is the structurally simplest compound, FeSe, which exhibits a tetragonal to orthorhombic structural phase transition at $T_S \sim 90$ K without concomitant spin density wave order and becomes superconducting below $T_c \sim 9$ K. Below T_S, the material exhibits strong electronic anisotropy, and the absence of tetragonal symmetry-breaking spin density wave order makes FeSe ideal for studying the origin and consequences of nematicity, i.e., the breaking of rotational symmetry while preserving translational symmetry. For example, an early scanning tunneling microscopy study of FeSe films on a SiC substrate found highly elongated vortices and impurity states and an associated nodal superconducting gap [1], but until recently similar experiments on crystals were hampered by sample quality. Other remarkable properties of FeSe include the significant enhancement of the superconducting critical temperature T_c both under pressure [2] and for monolayers of FeSe grown on $SrTiO_3$ surfaces [3–5].

Recently, the study of bulk FeSe crystals has been revitalized by the growth of very clean samples [6] amenable to the study of low-energy properties by, e.g., nuclear magnetic resonance (NMR), transport, scanning tunneling microscopy, angular resolved photoemission spectroscopy (ARPES), and quantum oscillation (QO) experiments. Even though a consensus on the electronic bands has not yet been reached by ARPES [7–13], recent studies found that the Fermi surface (FS) above T_S consists of two small hole cylinders of mainly d_{xz}/d_{yz} character around the Γ-Z line. The hole bands are split by a sizable spin-orbit (SO) coupling of $\lambda_{\mathrm{Fe}} \simeq 20$ meV above the structural transition, and the hole FS evolves into a single elongated hole cylinder below T_S [10]. ARPES also finds an electron pocket at the M point of mainly d_{xz}/d_{yz} character. Importantly, the expected d_{xz}/d_{yz} degeneracy at M is lifted by $\sim$50 meV, constituting strong evidence for orbital order in FeSe. We emphasize that these results for the electronic structure are very different from those obtained within density-functional theory (DFT) calculations [8,14]. For example, ARPES finds that the electronic bands in FeSe are renormalized compared to DFT calculations by a factor of $\sim$3 for the d_{xz}/d_{yz} bands and $\sim$9 for the d_{xy} band [8,10]. QOs performed at low T in magnetic fields large enough to suppress superconductivity are consistent with the ARPES data in observing small, largely 2D pockets, even though the amount of dispersion along k_z remains unsettled [10,15].

Recent ^{77}Se NMR measurements on FeSe have reported a clear splitting of the NMR line shape setting in at T_S, with an order parameterlike T dependence below T_S [16]. At high T, the spin-lattice relaxation rate is, however, unaffected by the structural transition, and it only exhibits a clear upturn at low T closer to the superconducting T_c [16,17]. These recent experiments have been interpreted as evidence for orbitally driven nematic behavior in FeSe, but despite the apparent weakness of (momentum summed) spin fluctuations near T_S, the spin-nematic picture may still apply. One possibility is that, unlike other FeSCs, fluctuations in FeSe with different wave vectors compete to frustrate long-range magnetic order [18].

Finally, we note that the resulting Fermi energy of the bands of FeSe seen by ARPES are remarkably small, comparable to the superconducting gap, which suggests the possibility that FeSe may be close to BEC/BCS crossover and may thus exhibit unusual thermodynamic

properties and magnetic field effects [19]. Thus, for multiple reasons, it is important to perform new theoretical studies of this intriguing material and to obtain a minimal model capturing its main electronic properties.

Here, we perform a theoretical study of the consequences of orbital order in a band relevant to FeSe. Starting from the DFT-generated band for FeSe obtained by Eschrig *et al.* [14], we apply band renormalization of $H_{\mathrm{TB}} = H_0/z$ (where $z = 6$ is renormalization factor and H_0 is the unrenormalized tight-binding Hamiltonian) and additional shifts to the hopping integrals [see the Supplemental Material [20] for details] to generate a new tight-binding model. We find that a band consistent with ARPES and QO is only possible in the presence of an orbital splitting setting in at T_S, and a T independent SO coupling. Further, we explain the recent Knight shift and the spin-relaxation rate measurements, and we study how a spin-fluctuation-mediated pairing can lead to a nodal gap structure in agreement with the measured density of states (DOS) and penetration depth λ of FeSe.

The bare Hamiltonian used in this study is given by

$$H = H_{\mathrm{TB}} + H_{\mathrm{OO}}, \tag{1}$$

$$H_{\mathrm{TB}} = \sum_{\mathbf{k},\mu,\nu,\sigma} t_{\mu\nu}(\mathbf{k}) c^{\dagger}_{\mu\sigma}(\mathbf{k}) c_{\nu\sigma}(\mathbf{k}), \tag{2}$$

$$H_{\mathrm{OO}} = \Delta_s(T) \sum_{\mathbf{k}\sigma} [n_{xz\sigma}(\mathbf{k}) - n_{yz\sigma}(\mathbf{k})]. \tag{3}$$

Here (μ, ν) are orbital indices, $t_{\mu\nu}(\mathbf{k})$ are the hopping integrals, and $n_{\mu\sigma}(\mathbf{k}) = c^{\dagger}_{\mu\sigma}(\mathbf{k}) c_{\mu\sigma}(\mathbf{k})$. All details of the hopping integrals are provided in the Supplemental Material [20] for both a five-orbital and a ten-orbital model. In the orbitally ordered state, H_{OO} contributes and $\Delta_s(T)$ is assumed to exhibit a mean-field T dependence with a maximum amplitude $\Delta_s(T = 0) = 50$ meV, see Fig. 1(b), inset. For simplicity, we focus in the main part of this Letter on a pure site-centered OO, but the consequences of an additional bond-centered OO of the form $\Delta_b(T) \sum_{\mathbf{k}\sigma} [\cos(k_x) - \cos(k_y)][n_{xz\sigma}(\mathbf{k}) + n_{yz\sigma}(\mathbf{k})]$ have also been studied; the results can be found in the Supplemental Material [20]. It has been reported by ARPES that the band splitting of the d_{xz}/d_{yz} bands at the M point in the orbitally ordered state does indeed show a mean-field behavior and saturates at low T with a band splitting of $\sim$50 meV [7,9,11,13]. Finally, we have included a SO term, $H_{\mathrm{SO}} = \lambda_{\mathrm{Fe}} \sum_i \sum_{x,y,z} L^{\alpha}_i S^{\alpha}_i$, which causes a band splitting of 20 meV in the tetragonal high T phase [21,22].

Band structure.—As shown in Figs. 1 and 2, the band structure and the resulting FS of our model is in nearly quantitative agreement with the experiments. Below T_S, the hole band at the Γ point is split by a 50 meV orbital order (at $T = 10$ K) and the bottom of the band lies $\sim$20 meV below

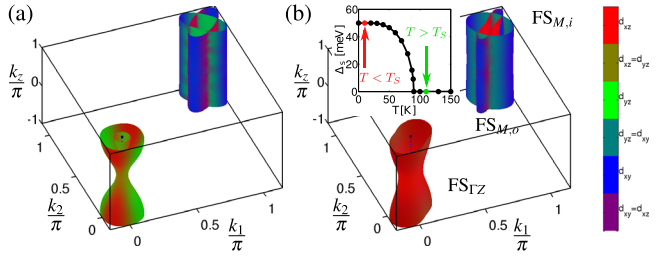

FIG. 1 (color online). (a) Fermi surface (FS) above T_S with SO coupling, and (b) FS at low T with an additional orbital splitting of 50 meV consisting of a Γ centered FS ($\mathrm{FS}_{\Gamma Z}$) cylinder and an inner and outer FS centered around the M point ($\mathrm{FS}_{M,i}$ and $\mathrm{FS}_{M,o}$). The inset shows the T dependence of the orbital splitting $\Delta_s(T)$; the two colored (gray) dots represent the T chosen for the two displayed FSs.

the chemical potential. Similarly, a dispersionless d_{xy} band is present at an energy of ~ -50 meV at the Γ point. At the M point, the electron pockets consist of quasi-2D cylinders where the outer pocket, with dominant d_{xy} character, encloses an inner d_{xz}/d_{yz} electron pocket. The inner electron band at the M point has an orbital splitting of 50 meV and almost grazes the Fermi level. These low T band structure values are in good agreement with the ARPES results [7,9–11,13].

Similar agreement with ARPES is achieved for $T > T_S$ where the orbital order is absent. There, the hole pockets consist of a quasi-2D outer circular cylinder and an inner hole pocket near the Z point, as seen in Fig. 1(a). The band also exhibits overall agreement with the orbital content observed in the polarized ARPES experiments [10]. At high T, the hole pocket at the zone center and the inner electron pocket at the M point contain both d_{xz} and d_{yz} character, and the outer electron pocket is predominantly of d_{xy} character. Similar orbital content of the Fermi pockets has also been seen in the ARPES measurements [9–12]. At low T, the orbital content of the hole cylinder is dominated by d_{xz} character (d_{yz} for the other twin). For a pure on-site ferro orbital order, both the hole and the inner electron cylinders have dominant d_{xz} orbital character [see Fig. 1(b)], whereas in the presence of an additional bond centered orbital order the electron cylinder can have the opposite d_{yz} orbital character [20]. For the electron pocket at low T, the inner pocket contains both d_{xz} and d_{yz} orbital character whereas the outer pocket at low T has orbital content dominated by the d_{xy} orbital. Although the orbital content of the electron pockets agrees well with the experiments [10–12], the outer d_{xy} electron pocket is difficult to observe in ARPES due to matrix element effects.

Quantum oscillations.—The extremal FS areas in FeSe at low T as well as their k_z dispersion have been studied by QO measurements [10,15,23]. These experiments have found four well separated QO frequencies, and arguments have been put forward that the QO frequencies correspond to one electron and one hole quasi-2D FS cylinder [15], as

well the possibility of a single quasi-2D hole cylinder and two almost dispersionless electron cylinders [10]. Although the former possibility cannot be ruled out, in this study we have pursued the latter possibility, which is supported by the weak k_z dispersion observed for the electron cylinders [10].

Starting from the ten-orbital tight-binding Hamiltonian and including the effects of SO coupling, we calculate the eigenenergies $\xi_i(\mathbf{k})$ on a grid in the Brillouin zone (BZ) and obtain the extremal areas F of the FS for cuts on planes perpendicular to the external magnetic field using a numerical method [24,25]. The direction of the magnetic field is then parametrized by the angle θ between the crystallographic c axis and the field direction. For $\theta = 0$, the electron pockets have extremal areas of $F \sim 588$ T for the d_{xy} pocket and $F \sim 102$ T for the smaller d_{xz}/d_{yz} pocket, as seen in Fig. 2(b). The hole Fermi cylinder is elongated due to the effect of orbital ordering with a maximum area of $F \sim 691$ T for $k_z = \pi$ and a minimum area of $F \sim 260$ T at $k_z = 0$. Overall, the experimentally observed binding energies for the d_{xz}/d_{yz} and d_{xy} bands, the 3D FS structure of both hole and electron pockets, and the extremal orbit areas as well as their k_z dispersion are in good agreement with our calculations. We have also calculated the Sommerfeld coefficient from the

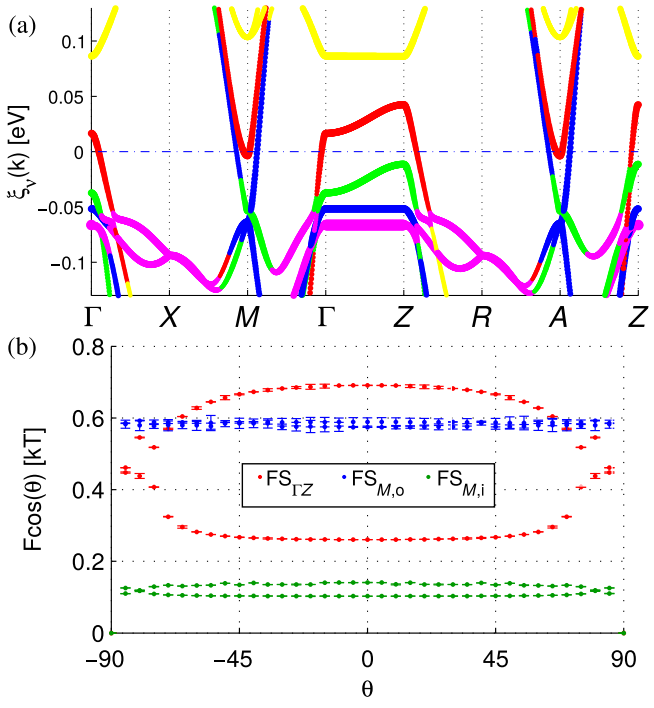

FIG. 2 (color online). (a) Band structure of the ten-orbital model at low T with orbital order and SO coupling, yielding the QO frequencies as a function of the magnetic field angle θ shown in (b), where the error bars indicate the numerical uncertainty in the determination of the extremal orbits. The orbital character in the band plot is indicated by the colors red (d_{xz}), green (d_{yz}), blue (d_{xy}), yellow ($d_{x^2-y^2}$), and purple ($d_{3z^2-r^2}$).

effective masses extracted from our quantum oscillation calculation. Using the numerically calculated effective masses together with the prescription given in Ref. [10], we find a Sommerfeld coefficient of 4.5 mJ/mol K^2, in reasonable agreement with the experimental value of ~5.3–5.7 mJ/mol K^2 [17,26,27].

Nuclear magnetic resonance.—Next, we test our electronic model of FeSe to see if it can also reproduce the NMR experiments [16,17]. For computational simplicity, in the following we apply the five-orbital model that shows good agreement with the ten-orbital model [20] and ignore the effect of SO coupling, which causes only small quantitative changes to the observables discussed in the remainder of this Letter. The NMR Knight shift is proportional to the homogeneous susceptibility, $K = A_{hf}\chi_{\mathrm{RPA}}(\mathbf{q} = 0) + K_{\mathrm{chem}}$, where we have approximated the spin susceptibility by its standard RPA form, A_{hf} is the hyperfine form factor, and K_{chem} is a T independent chemical shift which we have ignored for the purposes of this study. For the following calculations, we include local Coulomb interactions via the standard Hubbard-Hund Hamiltonian [28] parametrized by the Hubbard interaction Uz (z is the band renormalization) and the Hund's exchange J [20], calculate the orbitally resolved noninteracting susceptibility, and include interactions within RPA [29].

In the paramagnetic state, the form factor is a diagonal matrix with components $(A_{hf}^{xx}, A_{hf}^{yy}, A_{hf}^{zz})$ where the coordinates point along the Fe-Fe direction representing the magnetic field orientation of the NMR experiment. The form factor maintains the symmetry of the underlying lattice such that for the high T tetragonal phase, $A_{hf}^{xx} = A_{hf}^{yy} \neq A_{hf}^{zz}$, whereas the orbital ordered orthorhombic phase has $A_{hf}^{xx} \neq A_{hf}^{yy} \neq A_{hf}^{zz}$. This anisotropy leads to a split Knight shift frequency below T_S in twinned samples of FeSe [16,17].

As shown by Baek *et al.*, [16], the Knight shift splitting exhibits a T dependence proportional to the mean-field orbital order parameter. Therefore, we model the form factor by the expression $A_{hf} = \alpha \pm g(T)$, where $g(T) = \beta\Delta_s(T)$, (α, β) are fitting parameters, and $\pm$ refers to the two orthorhombic domains l_1 and l_2. The calculated Knight shift as a function of T is shown in Fig. 3(a). At high T above T_S, the Knight shift increases with T similar to the experiments, in contrast to the DFT-generated nonrenormalized bands [20]. Below T_S, for a particular magnetic field direction, the Knight shift shows a minimum value around $T \sim 60$ K similar to the experimental results. Below $T \sim 60$ K, we find a slight enhancement of the Knight shift signal. Although the measured Knight shift saturates and does not show this enhancement for both orthorhombic domains, this may be simply related to a deviation of the splitting from mean-field behavior found experimentally at the lowest T [16].

In order to study the evolution of the spin fluctuations, we have also calculated the spin-lattice relaxation rate

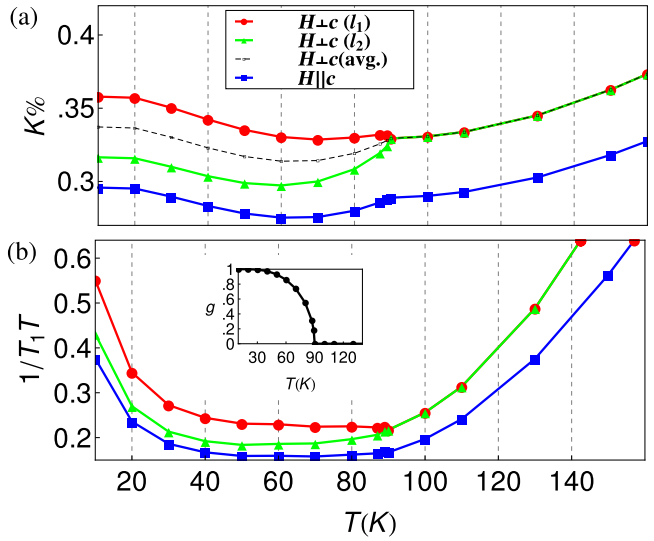

FIG. 3 (color online). (a) NMR Knight shift versus T. The hyperfine form factor has been taken as $A_{hf}^{l_1/l_2} = 0.6[0.57 \pm 0.035g(T)]$ for $H \perp c$ and $A_{hf}^{c} = 0.6 \times 0.5$ for $H \| c$. (b) Spin-lattice relaxation rate versus T with $A_{hf}^{l_1/l_2} = 0.57 \pm 0.035g(T)$ for $H \perp c$ and $A_{hf} = 0.5$ for $H \| c$. Red curve $H \perp c$ (domain l_1), green curve $H \perp c$ (domain l_2), black curve $H \perp c$ (domain average), and blue curve $H \| c$.

$$\frac{1}{T_1 T} = \lim_{\omega_0 \to 0} \frac{\gamma_N^2}{2N} k_B \sum_{\mathbf{q}\alpha\beta} |A_{hf}^{\alpha\beta}(\mathbf{q})|^2 \frac{\mathrm{Im}\{\chi_{\mathrm{RPA}}^{\alpha\beta}(\mathbf{q}, \omega_0)\}}{\hbar\omega_0}. \quad (4)$$

NMR experiments probing the ^{77}Se atoms in FeSe exhibit a q dependent hyperfine form factor in the paramagnetic state given by $A_{hf}^{\alpha\beta}(\mathbf{q}) = A_{hf}^{\alpha\beta} \cos(q_x/2) \cos(q_y/2)$, assuming that the Se ion interacts with its four nearest Fe neighbors only. Since ^{77}Se is a spin 1/2 ion, quadrupole-type coupling to local lattice distortions do not contribute to the relaxation rate. As seen from the form factor, spin fluctuations at the edges of the Brillouin zone will be filtered out. The result of the calculation for $1/T_1T$ for interaction parameters $Uz = 1.8$ eV and $Jz = 0.1Uz$ is shown in Fig. 3(b). As was seen, the spin fluctuations are enhanced at low T. However, as was observed in recent NMR experiments [16,17], the enhancement does not occur at T_S despite the sharp increase of Δ_s at T_S, but below about $T \sim 40$ K. Interestingly, this increase of spin fluctuations at low T is caused by the orbital ordering which leads to a low T incommensurability in the spin susceptibility that pushes spectral weight away from the BZ edges, and therefore does not allow the structure factor to effectively filter out those fluctuations [20]. Note that although the low T spin susceptibility avoids the magnetic state by remaining below the Stoner limit, the enhanced fluctuations at low T have important consequences for spin-fluctuation-mediated pairing.

Spin-fluctuation pairing.—What is the dominant pairing instability for the low T orbitally ordered state? To answer this question, we consider the scattering vertex in the singlet channel projected onto the band space $\Gamma(\mathbf{k}, \mathbf{k}')$ [20] and solve the linearized gap equation

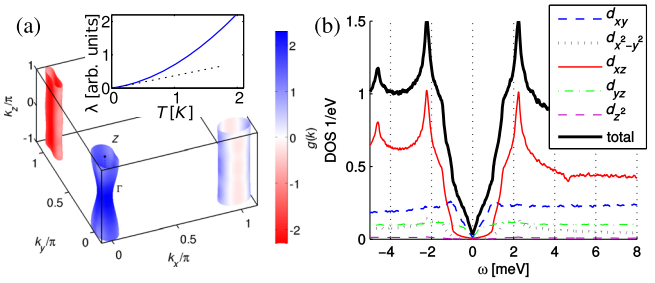

FIG. 4 (color online). Superconducting order parameter as calculated from a spin-fluctuation pairing using the interactions $Uz = 1.8$ eV and $Jz = 0.1Uz$ shows nodal regions on one of the electron pockets (a). The corresponding DOS clearly exhibits nodal behavior (b) and the penetration depth λ stays linear down to low T in agreement with the experiments [(a), inset].

$$-\frac{1}{V_G} \sum_j \int_{\mathrm{FS}_j} dS' \Gamma(\mathbf{k}, \mathbf{k}') \frac{g_\alpha(\mathbf{k}')}{|v_{\mathrm{F}j}(\mathbf{k}')|} = \lambda_\alpha g_\alpha(\mathbf{k}), \quad (5)$$

where $v_{\mathrm{F}j}(\mathbf{k}')$ is the Fermi velocity of band j and the integration is performed over FS_j to obtain the gap symmetry functions $g_\alpha(\mathbf{k})$ and the set of eigenvalues λ_α. The largest eigenvalue corresponds to the leading instability and the corresponding eigenfunction determines the structure of the superconducting gap $\Delta(\mathbf{k}) \sim g(\mathbf{k})$ close to T_c. In order to solve Eq. (5), the FS is discretized using a Delaunay triangulation [22] such that it reduces to solving a matrix eigenvalue problem. In the absence of orbital order, the leading instability is d wave, with nodes on the hole pockets and no accidental nodes on the electron pockets, whereas in the absence of any band renormalization the leading instability is a nodeless sign changing $s\pm$ state. In Fig. 4(a) we show the result for the gap structure in the low T phase with orbital order. The character of the gap structure cannot be classified in s-or d-wave symmetry because the underlying band structure is only C_2 symmetric [30]. As seen in Fig. 4(a), the orbital order has strong effects on the position of the nodes; i.e., it removes the nodes from the hole pockets and induces nodal lines on the X-centered (Y for the other twin) electron pocket. The associated DOS (maximum gap set to $\approx$2.2 meV) and the linear-T behavior of the low T penetration depth λ shown in Fig. 4 are remarkably similar to recent experimental findings [1,19].

In summary, we have presented a model for the electronic structure of FeSe that includes orbital ordering, which is consistent with recent ARPES and QO experiments on high quality FeSe samples. This band, along with the standard local interaction potentials and exchanges, explains both the T dependence of the NMR Knight shifts and spin-relaxation rate, and it leads to a pairing state with

nodes and a T dependence of the London penetration depth in agreement with a series of recent experiments on FeSe.

We acknowledge our useful discussions with B. Büchner, A. Böhmer, A. Coldea, T. Hanaguri, F. Hardy, M. Lang, I. I. Mazin, C. Meingast, T. Shibauchi, and R. Valenti. We thank D. Guterding for the use of his QO code [31]. A. K. and B. M. A. acknowledge financial support from a Lundbeckfond fellowship (Grant No. A9318). P. J. H. was partially supported by U.S. DOE Grant No. DEFG02-05ER46236. This research was supported in part by the KITP under NSF Grant No. PHY11-25915.

[1] C.-L. Song, Y.-L. Wang, P. Cheng, Y.-P. Jiang, W. Li, T. Zhang, Z. Li, K. He, L. Wang, J.-F. Jia, H.-H. Hung, C. Wu, X. Ma, X. Chen, and Q.-K. Xue, Science **332**, 1410 (2011).

[2] S. Medvedev, T. M. McQueen, I. A. Troyan, T. Palasyuk, M. I. Eremets, R. J. Cava, S. Naghavi, F. Casper, V. Ksenofontov, G. Wortmann, and C. Felser, Nat. Mater. **8**, 630 (2009).

[3] W. Qing-Yan *et al.*, Chin. Phys. Lett. **29**, 037402 (2012).

[4] S. Tan, Y. Zhang, M. Xia, Z. Ye, F. Chen, X. Xie, R. Peng, D. Xu, Q. Fan, H. Xu, J. Jiang, T. Zhang, X. Lai, T. Xiang, J. Hu, B. Xie, and D. Feng, Nat. Mater. **12**, 634 (2013).

[5] J.-F. Ge, Z.-L. Liu, C. Liu, C.-L. Gao, D. Qian, Q.-K. Xue, Y. Liu, and J.-F. Jia, Nat. Mater. **14**, 285 (2015).

[6] A. E. Böhmer, F. Hardy, F. Eilers, D. Ernst, P. Adelmann, P. Schweiss, T. Wolf, and C. Meingast, Phys. Rev. B **87**, 180505 (2013).

[7] K. Nakayama, Y. Miyata, G. N. Phan, T. Sato, Y. Tanabe, T. Urata, K. Tanigaki, and T. Takahashi, Phys. Rev. Lett. **113**, 237001 (2014).

[8] J. Maletz, V. B. Zabolotnyy, D. V. Evtushinsky, S. Thirupathaiah, A. U. B. Wolter, L. Harnagea, A. N. Yaresko, A. N. Vasiliev, D. A. Chareev, A. E. Böhmer, F. Hardy, T. Wolf, C. Meingast, E. D. L. Rienks, B. Büchner, and S. V. Borisenko, Phys. Rev. B **89**, 220506 (2014).

[9] T. Shimojima, Y. Suzuki, T. Sonobe, A. Nakamura, M. Sakano, J. Omachi, K. Yoshioka, M. Kuwata-Gonokami, K. Ono, H. Kumigashira, A. E. Böhmer, F. Hardy, T. Wolf, C. Meingast, H.v. Löhneysen, H. Ikeda, and K. Ishizaka, Phys. Rev. B **90**, 121111 (2014).

[10] M. D. Watson, T. K. Kim, A. A. Haghighirad, N. R. Davies, A. McCollam, A. Narayanan, S. F. Blake, Y. L. Chen, S. Ghannadzadeh, A. J. Schofield, M. Hoesch, C. Meingast, T. Wolf, and A. I. Coldea, Phys. Rev. B **91**, 155106 (2015).

[11] P. Zhang, T. Qian, P. Richard, X. P. Wang, H. Miao, B. Q. Lv, B. B. Fu, T. Wolf, C. Meingast, X. X. Wu, Z. Q. Wang, J. P. Hu, and H. Ding, arXiv:1503.01390.

[12] Y. Suzuki, T. Shimojima, T. Sonobe, A. Nakamura, M. Sakano, H. Tsuji, J. Omachi, K. Yoshioka, M. Kuwata-Gonokami, T. Watashige, R. Kobayashi, S. Kasahara, T. Shibauchi, Y. Matsuda, Y. Yamakawa, H. Kontani, and K. Ishizaka, arXiv:1504.00980.

[13] Y. Zhang, M. Yi, Z.-K. Liu, W. Li, J. J. Lee, R. G. Moore, M. Hashimoto, N. Masamichi, H. Eisaki, S.-K. Mo, Z. Hussain, T. P. Devereaux, Z.-X. Shen, and D. H. Lu, arXiv:1503.01556.

[14] H. Eschrig and K. Koepernik, Phys. Rev. B **80**, 104503 (2009).

[15] T. Terashima, N. Kikugawa, A. Kiswandhi, E.-S. Choi, J. S. Brooks, S. Kasahara, T. Watashige, H. Ikeda, T. Shibauchi, Y. Matsuda, T. Wolf, A. E. Böhmer, F. Hardy, C. Meingast, H.v. Löhneysen, M.-T. Suzuki, R. Arita, and S. Uji, Phys. Rev. B **90**, 144517 (2014).

[16] S.-H. Baek, D. V. Efremov, J. M. Ok, J. S. Kim, J. van den Brink, and B. Büchner, Nat. Mater. **14**, 210 (2015).

[17] A. E. Böhmer, T. Arai, F. Hardy, T. Hattori, T. Iye, T. Wolf, H.v. Löhneysen, K. Ishida, and C. Meingast, Phys. Rev. Lett. **114**, 027001 (2015).

[18] J. K. Glasbrenner, I. I. Mazin, H. O. Jeschke, P. J. Hirschfeld, and R. Valentí, arXiv:1501.04946.

[19] S. Kasahara, T. Watashige, T. Hanaguri, Y. Kohsaka, T. Yamashita, Y. Shimoyama, Y. Mizukami, R. Endo, H. Ikeda, K. Aoyama, T. Terashima, S. Uji, T. Wolf, H. von Löhneysen, T. Shibauchi, and Y. Matsuda, Proc. Natl. Acad. Sci. U.S.A. **111**, 16309 (2014).

[20] See Supplemental Material at http://link.aps.org/supplemental/10.1103/PhysRevLett.115.026402 for technical details regarding the tight-binding model used in this Letter, the Hubbard-Hund Hamiltonian taken into account for the pairing calculation and the calculation of the NMR relaxation rate. We also provide results assuming additionally a d-wave orbital order.

[21] J. Friedel, P. Lenglart, and G. Leman, J. Phys. Chem. Solids **25**, 781 (1964).

[22] A. Kreisel, Y. Wang, T. A. Maier, P. J. Hirschfeld, and D. J. Scalapino, Phys. Rev. B **88**, 094522 (2013).

[23] A. Audouard, F. Duc, L. Drigo, P. Toulemonde, S. Karlsson, P. Strobel, and A. Sulpice, Europhys. Lett. **109**, 27003 (2015).

[24] P. Rourke and S. Julian, Comput. Phys. Commun. **183**, 324 (2012).

[25] J. Diehl, S. Backes, D. Guterding, H. O. Jeschke, and R. Valentí, Phys. Rev. B **90**, 085110 (2014).

[26] J.-Y. Lin, Y. S. Hsieh, D. A. Chareev, A. N. Vasiliev, Y. Parsons, and H. D. Yang, Phys. Rev. B **84**, 220507 (2011).

[27] M. Abdel-Hafiez, Y.-Y. Zhang, Z.-Y. Cao, C.-G. Duan, G. Karapetrov, V. M. Pudalov, V. A. Vlasenko, A. V. Sadakov, D. A. Knyazev, T. A. Romanova, D. A. Chareev, O. S. Volkova, A. N. Vasiliev, and X.-J. Chen, Phys. Rev. B **91**, 165109 (2015).

[28] K. Kuroki, S. Onari, R. Arita, H. Usui, Y. Tanaka, H. Kontani, and H. Aoki, Phys. Rev. Lett. **101**, 087004 (2008).

[29] S. Graser, T. A. Maier, P. J. Hirschfeld, and D. J. Scalapino, New J. Phys. **11**, 025016 (2009).

[30] J. Kang, A. F. Kemper, and R. M. Fernandes, Phys. Rev. Lett. **113**, 217001 (2014).

[31] See https://github.com/danielguterding/dhva.